# Electrical Modeling of Electrolyzers

Ushnish Chowdhury
*Department of Electrical Engineering and Automation*
*Aalto University, Finland*
ushnish.chowdhury@aalto.fi

***Abstract*—This paper introduces a comprehensive electrical model tailored for water electrolyzers. The proposed model captures the temperature and pressure-dependent characteristics of these electrochemical devices, while also accounting for nonlinearities arising from irreversible overvoltage losses and dynamic, capacitive behavior associated with the double-layer effect. Additionally, the frequency response of the model is analyzed to facilitate the linearization of the electrolyzer's overall impedance. Finally, simulation results are presented to evaluate the model's applicability in representing the operational behavior of electrolyzers.**

***Index Terms*—Water electrolyzers, electrical modeling, linearization, renewable energy**

## I. Introduction

Hydrogen serves as a highly efficient energy carrier, particularly in energy-intensive sectors that are hard to electrify [1], [2]. These include long-distance transportation modes such as aviation and maritime shipping, as well as industrial processes like steel manufacturing and glass production. Hydrogen also plays a crucial role as a key feedstock in various chemical synthesis processes, including the production of ammonia and methane, which are fundamental to numerous industrial applications. For instance, ammonia is widely utilized in the manufacture of fertilizers essential for modern agriculture, while methane derivatives serve as precursors in the production of soaps, detergents, and other chemical products. Beyond these, hydrogen's role extends to the synthesis of methanol and other chemicals that form the backbone of industries such as pharmaceuticals, plastics, and textiles. However, 99% of hydrogen production currently relies on processes such as steam methane reforming and natural gas reforming, both of which contribute significantly to carbon emissions [1], [3], [4]. It is, therefore, crucial to explore alternative approaches for hydrogen production that minimize carbon emissions.

Green hydrogen technology has been recognized as a viable alternative capable of producing hydrogen with a zero-carbon footprint across all phases of its production process. The methodology uses electrochemical devices called electrolyzers, employ electricity generated from renewable energy sources to split water molecules into hydrogen ($H_2$) and oxygen without producing emissions at any stage. Recognizing the advantages of green hydrogen, international organizations and governing bodies are formulating strategies to transition away from the predominantly used methods of hydrogen production [1], [5]. The European Union, for example, has exhibited a strong commitment in advancing green hydrogen as a key element in its energy transition strategy, with the objective to scale up production up to 10 million tonnes by the start of 2030 [2].

As electrolyzers emerge as key enablers in the global effort to reduce carbon emissions, it is essential to thoroughly understand their electrical behavior to ensure effective integration into the grid. Electrolyzers, being electrochemical devices, nonlinear and dynamic characteristics that should be accounted for under varying operational conditions, such as fluctuations in temperature, pressure, and current [6]–[10]. A comprehensive electrical model is, therefore, crucial in capturing these phenomena and also enables the linearization of the system for specific conditions required for integrating them to the power grid.

The paper begins by providing an overview of the fundamentals of water electrolysis and the various types of electrolyzers in Section II. Section III introduces the proposed electrical model, with a detailed explanation of each component to illustrate the behavior of an electrolyzer. In Section IV, the focus shifts to linearizing the overall electrolyzer impedance to facilitate further analysis. Finally, simulation results obtained using PLECS are presented and compared with findings from referenced literature as a proof of validation for the model.

## II. Basics of water electrolysis

Water electrolysis is the process involving the application of an electric current, which facilitates the separation of water into its gaseous products through redox reactions at the two electrodes (anode and cathode), thereby enabling the efficient production of these gases. The general process has been depicted in Fig. 1. The fundamental chemical reaction governing electrolysis is

$$\mathrm{H_2O\,(l)} \longrightarrow \mathrm{H_2(g)} + \frac{1}{2}\,\mathrm{O_2(g)} \tag{1}$$

Electrolysis is further distinguished based on the type of electrolyte used, which modifies the half-cell reactions at each electrode. Alkaline water electrolysis (AWE) utilizes an alkaline solution consisting water and potassium hydroxide or sodium hydroxide, facilitating the movement of hydroxide

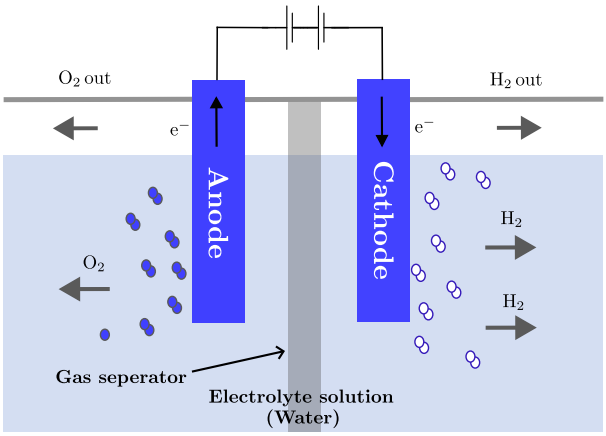


Fig. 1: General water electrolysis.

ions.

$$2\,H_2O\,(l) + 2\,e^- \rightleftharpoons H_2(g) + 2\,OH^-(aq) \tag{2a}$$

reduction at cathode

$$2\,OH^-(aq) + 2\,e^- \rightleftharpoons \frac{1}{2}\,O_2(g) + H_2O\,(l) + 2\,e^- \tag{2b}$$

oxidation at anode

A proton membrane exchange water electrolysis (PEMWE) system employs a solid polymer electrolyte (typically perfluoroalkylsulfonic acid [11]) which allows proton transport, separates the gaseous products, and provides a layer of insulation for the electrodes. The solution used for this process contains minimal impurities, thus generating purer $H_2$ gas when compared to AWE.

$$2\,H^+(aq) + 2\,e^- \rightleftharpoons H_2(g) \tag{3a}$$

reduction at cathode

$$H_2O\,(l) \rightleftharpoons \frac{1}{2}\,O_2(g) + 2\,H^+(aq) + 2\,e^- \tag{3b}$$

oxidation at anode

While PEMWE offers significant advantages in efficiency and produces hydrogen of higher purity and compact stack size, the overall costs associated with developing and maintaining a PEMWE system are considerable. This high expense is primarily due to the reliance on precious metals, including platinum and iridium, for the catalyst layers, along with nickel for additional system components [12]. Ultimately, the decision between AWE and PEMWE for large-scale hydrogen production will depend on the specific requirements and constraints of the particular application.

Other electrolysis methods, such as solid-oxide water electrolysis and anion exchange membrane water electrolysis, are currently subjects of active research and development. Efforts are focused on optimizing these technologies to achieve more favorable and practical operating conditions [13]. Since these technologies have not yet reached commercialization and remain largely in the research and development phase, unlike the more established AWE and PEMWE, they are excluded from this study.

## III. Electrical Model of Electrolyzers

The operational principles of electrolyzers are grounded in Faraday's first law of electrolysis, which states that the amount of chemical change at the electrode-electrolyte interface is directly proportional to the amount of electricity passed through the system [10].

$$\frac{dn_{H_2}}{dt} = \eta\frac{jA}{n_e F} = \eta\frac{i_E}{n_e F} \tag{4}$$

where $\frac{dn_{H_2}}{dt}$ is the rate of production of hydrogen molecules, $\eta$ is the efficiency of the supplied current, $j$ is the current density, $A$ is the active surface area, $i_E = jA$, is the current flowing through the electrolyzer, $n_e$ refers to the number of electrons involved in the production of a single hydrogen molecule, which is always two incase of water electrolysis and $F = 9.65 \cdot 10^4$ C/mol is the Faraday's constant.

In real-world systems, the efficiency, $\eta$ is rarely unity and is reduced by factors such as stray currents and nonlinearities resulting from gas crossover through the gas separator [10]. An overall voltage can be determined by considering the various phenomena occurring within an electrolyzer, including these nonlinearities and losses [6]–[10].

$$u_E = u_{rev} + u_{ohm} + u_{act} \tag{5}$$

where $u_{rev}$ is the reversible voltage, the minimum voltage required to initiate the electrolysis process, $u_{ohm}$ refers to the ohmic losses in each cell, and $u_{act}$ is the overall activation voltage produced due to kinetic losses in both cathode and anode. All terms have been elaborated upon in the subsequent subsections III-A, III-B and III-C. Fig. 2 shows the comprehensive equivalent electrical circuit for alkaline or proton exchange membrane (PEM) electrolyzers is modelled by incorporating all phenomena outlined in (5), including the various resistive and capacitive components that represent the electrochemical reactions.

### A. Reversible voltage

The reversible voltage, $u_{rev}$, in electrolysis, refers to the theoretical voltage at which an electrochemical reaction proceeds with no energy losses. In this ideal scenario, the system operates with perfect thermodynamic efficiency, characterized by zero entropy generation and the complete conversion of energy without any dissipation. The total reversible voltage in a electrolyzer cell is calculated by combining the half reactions at both electrodes

$$u_{rev} = u_{rev,an} - u_{rev,ca} \tag{6}$$

where subscripts an and ca represent anode and cathode respectively. The reversible voltage for both electrodes are

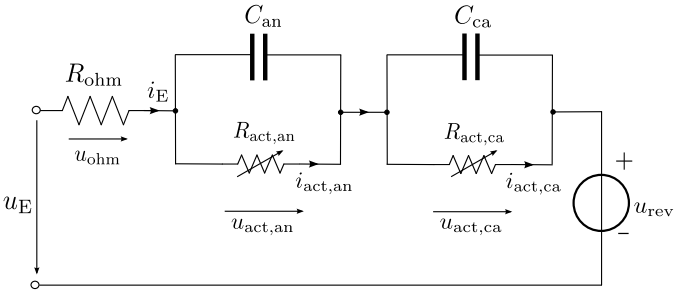


Fig. 2: Electrical equivalent circuit of an electrolyzer stack.

therefore obtained through the implementation of Nerst equation.

$$u_{\text{rev,an}} = u^0_{\text{rev,an}} + f(T)\ln\frac{a^{1/2}_{\text{O}_2}a^2_{\text{H}^+}}{a_{\text{H}_2\text{O}}} \tag{8a}$$

$$u_{\text{rev,ca}} = u^0_{\text{rev,ca}} + f(T)\ln\frac{a^2_{\text{H}^+}}{a_{\text{H}_2}} \tag{8b}$$

$$f(T) = \frac{\bar{R}T}{n_{\text{e}}F} \tag{8c}$$

where $\bar{R} = 8.314\ \text{Jmol}^{-1}\text{K}^{-1}$ is the universal gas constant and $a_{\text{O}_2}$, $a_{\text{H}_2\text{O}}$, $a_{\text{H}^+}$ and $a_{\text{H}_2}$ are the specific activities of the chemical reagents. The parameter $u^0_{\text{rev,an}}$ and $u^0_{\text{rev,ca}}$ are the initial reversible voltage at standard pressure (1 bar) as a function of temperature at both anode and cathode respectively. The overall reaction is

$$u_{\text{rev}} = u^0_{\text{rev}} + f(T)\ln\frac{a^2_{\text{H}_2}a^{1/2}_{\text{O}_2}}{a_{\text{H}_2\text{O}}} \tag{9}$$

The standard reversible voltage $u^0_{\text{rev}}$ has been derived utilizing various linear and polynomial approximations, and experimental equations. All of the equations exhibit minimal differences in output when operated within the designated temperature range [10]. The activity of an ideal gas can be thermodynamically defined as a measure of the effective concentration of a species within a mixture. It is therefore expressed as a ratio of the partial pressure of the gas to a reference pressure, commonly selected as $p^0 = 1\,\text{bar}$.

After applying all of the mentioned equations, the final reversible voltage for an alkaline electrolyzer becomes

$$u_{\text{rev}} = u^0_{\text{rev}} + f(T)\ln\frac{(p - p_{\text{sv,el}}(T,m))^{3/2}p_{\text{sv}}(T)}{(p^0)^{3/2}p_{\text{sv,el}}(T,m)} \tag{10}$$

where $p$ is the system pressure, $p_{\text{sv}}$ is the saturated vapour pressure of water and $p_{\text{sv,el}}$ is the saturated vapour pressure of the electrolyte, dependent on temperature and molality.

In contrast to alkaline electrolyzers, the pressures at the two electrodes in a PEM electrolyzer are not equal and must therefore be accounted for separately in the reversible voltage equation.

$$u_{\text{rev}} = u^0_{\text{rev}} + f(T)\ln\frac{(p_{\text{ca}} - p_{\text{sv}}(T))(p_{\text{an}} - p_{\text{sv}}(T))^{1/2}}{(p^0)^{3/2}} \tag{11}$$

where $p_{\text{an}}$ and $p_{\text{ca}}$ are pressure of the anode and cathode respectively.

Although Equations (10) and (11) differ significantly, both yield a reversible voltage value o $1.229\,\text{V}$ under standard conditions of $25\,^\circ\text{C}$ and 1 bar pressure [7], [8], [10]. As shown in Fig. 2, the reversible voltage can be modeled to be voltage source dependent on operating temperature and pressure.

### *B. Ohmic overvoltage*

The flow of electrons and ions through the electrodes (anode and cathode), diaphragm, bipolar plates, and current collectors face resistance, resulting in the ohmic overvoltage, $u_{\text{ohm}}$ in the electrolyzer. The overvoltage increases linearly following Ohm's law as the current flowing through the electrolyzer stack ($i_{\text{E}}$) increases [7]. In Fig. 2, it is represented as a basic resistor.

$$u_{\text{ohm}} = i_{\text{E}}R_{\text{ohm}} \tag{12}$$

where $R_{\text{ohm}}$ is the total resistance for the electrolyzer stack. The resistance is expressed as a function of the operating temperature.

$$R_{\text{ohm}} = \frac{r}{A} \tag{13a}$$

$$r = r_1 + r_2T + \frac{r_3}{T} + \frac{r_4}{T^2} \tag{13b}$$

where $r$ is the area-specific resistance of the cell and $A$ is the total surface area of the cell. The parameter $r$ is further segregated as shown in (13b) where $r_1$, $r_2$, $r_3$ and $r_4$ are experimentally derived parameters, with the latter three being temperature-dependent. The term $r_2$ represents the resistance encountered by electron movement due to various cell components, such as electrodes and bipolar plates. While $r_3$ and $r_4$ are the ionic resistance caused by the electrolyte and the diaphragm. Thus $R_{\text{ohm}}$ is inversely proportional to the temperature, exhibiting behavior that is contrary to that of a typical resistor. Increase in temperature therefore can positively influence the electrolyzer performance by reducing the ohmic losses.

### *C. Activation overvoltage and double-layer effect*

Initialization of the formation of hydrogen and oxygen through the electrolysis process requires additional energy beyond the theoretical minimum reversible voltage necessary to overcome the energy barriers associated with the electrochemical reactions at the electrodes [7]. This additional energy accounts for the activation energy required to drive the reaction kinetics at the electrodes and the inherent inefficiencies present within the system [8]. The overvoltage resulting from such a phenomenon is known as the activation overvoltage, $u_{\text{act}}$ which occurs in both electrodes. In Fig. 2 it is presented as the voltage developed across the nonlinear resistors $R_{\text{act,an}}$ and $R_{\text{act,ca}}$.

The overvoltage can be approximated and expressed in an exponential form, as described in [6]–[8], [10].

$$\frac{i_{\text{E}}}{i^0_{\text{x}}} = \exp\left(\frac{\alpha n_{\text{e}}F}{\bar{R}T}u_{\text{act,x}}\right) \tag{14}$$

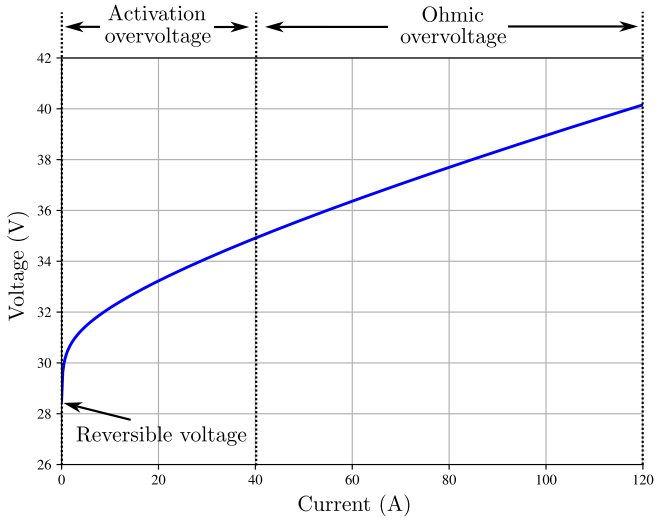


Fig. 3: Example $i-u$ curve of an alkaline electrolyzer

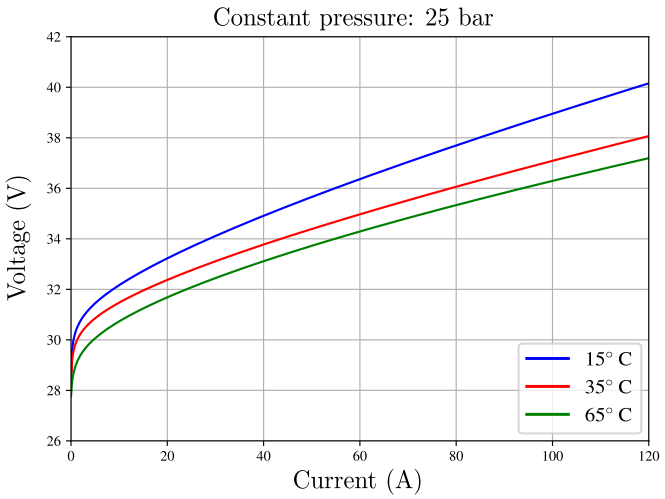


Fig. 4: Example $i-u$ characteristics of an alkaline electrolyzer

where $i_{\mathrm{x}}^{0}$ is the equilibrium current in the electrodes, $\alpha$ is the charge transfer coefficient ($\alpha \in [0,1]$). Subscript x represents either of the electrodes. Equivalent reciprocal form can be derived where the current is the input and voltage the output.

$$u_{\mathrm{act,x}} = \frac{\bar{R}T}{\alpha n_{\mathrm{e}} F} \ln \frac{i_{\mathrm{E}}}{i_{\mathrm{x}}^{0}} \tag{15}$$

Further adjustments can be made to deduce the relation between the constant terms $\bar{R}$, $n_{\mathrm{e}}$ and $F$ and the operating temperature in (15), modifying it to

$$u_{\mathrm{act,i}} = s_{\mathrm{x}} \ln \left( \frac{1}{t_{\mathrm{x}}} i_{act,\mathrm{x}} + 1 \right) \tag{16}$$

where $s_{\mathrm{x}}$ and $t_{\mathrm{x}}$ are those parameters derived from experimental data related to the cathode and anode (denoted by the subscript x) during the activation process. The term $s_{\mathrm{x}}$ directly influences the reaction rate as a function of temperature at the electrodes. A lower value of $s_{\mathrm{x}}$, corresponds to reduced activation losses. The term $t_{\mathrm{x}}$ is associated with the exchange currents at each electrode, and is inversely related to the activation losses, i.e. higher values of $t_{\mathrm{x}}$ reduce the activation losses for each electrode.

$$s_{\mathrm{x}} = s_{1,\mathrm{x}} + s_{2,\mathrm{x}} T + s_{3,\mathrm{x}} T^2 \tag{17a}$$

$$t_{\mathrm{x}} = t_{1,\mathrm{x}} + t_{2,\mathrm{x}} T + t_{3,\mathrm{x}} T^2 \tag{17b}$$

Thus, the overall activation overvoltage for the electrolyzer stack can be expressed as

$$u_{\mathrm{act}} = s_{\mathrm{an}} \ln \left( \frac{1}{t_{\mathrm{an}}} i_{\mathrm{act,an}} + 1 \right) + s_{\mathrm{ca}} \ln \left( \frac{1}{t_{\mathrm{ca}}} i_{\mathrm{act,ca}} + 1 \right) \tag{18}$$

As depicted in Fig. 2, two capacitors $C_{\mathrm{an}}$ and $C_{\mathrm{ca}}$ are connected in parallel with the nonlinear resistors to represent the electric double-layer (EDL) effect at each electrode. The phenomenon is formed at the interface between an electrode and electrolyte, making the electrolyzer behave like a dielectric during changes in rate of oxidation and reduction at the electrodes [8], [14]. The arrangement of ions in the EDL affects the transfer of electrons and ions during the electrochemical reactions, which directly influences the activation overvoltage. During dynamic operations the EDL therefore impacts how quickly the system responds [14].

A state-space representation of the electrolyzer is derived with nonlinear and dynamic effects taken into account. The dynamic behavior is expressed as

$$C_{\mathrm{an}} \frac{\mathrm{d}u_{\mathrm{act,an}}}{\mathrm{d}t} = i_{\mathrm{E}} - i_{\mathrm{act,an}}(u_{\mathrm{act,an}}) \tag{19a}$$

$$C_{\mathrm{ca}} \frac{\mathrm{d}u_{\mathrm{act,ca}}}{\mathrm{d}t} = i_{\mathrm{E}} - i_{\mathrm{act,ca}}(u_{\mathrm{act,ca}}) \tag{19b}$$

The resulting state-space representation of the electrolyzer stack voltage is

$$u_{\mathrm{E}} = R_{\mathrm{ohm}} i_{\mathrm{E}} + u_{\mathrm{act,an}} + u_{\mathrm{act,ca}} + u_{\mathrm{rev}} \tag{20}$$

Fig. 3 illustrates the nonlinear ii-uu characteristics of an alkaline electrolyzer, with the behavior further divided into sections contributing to this response. The curve begins at approximately 28 V, which is the reversible voltage. The nonlinear increase in voltage with current corresponds to the activation overvoltage, while the linear increase following the nonlinear behavior represents the ohmic overvoltage. These characteristics are directly influenced by the operating temperature and pressure. Fig. 4 shows that behavior, where the $i-u$ characteristics were determined at three different temperatures: 15°C, 35°C and 65°C, under a constant pressure of 25 bars. The results indicate that the overall electrolyzer voltage $u_{\mathrm{E}}$ decreases as the operating temperature increases.

## IV. Linearized Model

Linearization facilitates the analysis of complex nonlinear systems by approximating them with linear equations around a specific operating point. For electrolyzers, electrochemical impedance spectroscopy is applied to determine the equivalent electrical impedance [6], [8]. It allows for the investigation of

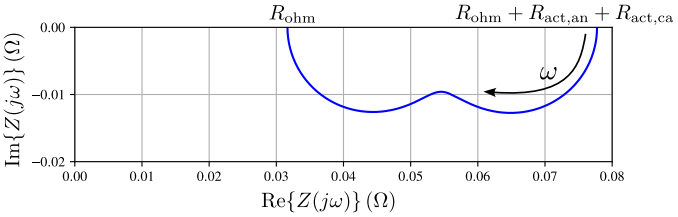


Fig. 5: Nyquist plot for the total electrolyzer impedance.

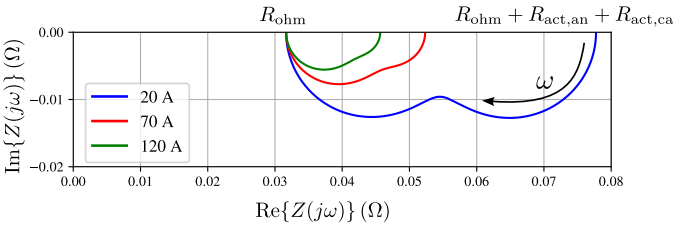


Fig. 6: Nyquist plot for the total electrolyzer impedance at three different currents.

TABLE I: Parameters used to plot Fig. 5

| | | | |
|---|---|---|---|
| $R_{\text{ohm}}$ | $0.032\,\Omega$ | | |
| $R_{\text{act,an}}$ | $0.023\,\Omega$ | $R_{\text{act,ca}}$ | $0.023\,\Omega$ |
| $C_{\text{an}}$ | $0.638\,\text{F}$ | $C_{\text{ca}}$ | $0.031\,\text{F}$ |

the charge transfer kinetics and mechanisms of a specific electrochemical process, in this case, the ionic movement between the electrodes and the electrolyte. Applying the linearization results in the impedance to be

$$\begin{aligned} \text{Z}(s) &= \frac{u_{\text{E}}(s)}{i_{\text{E}}(s)} \\ &= R_{\text{ohm}} + \frac{R_{\text{act,an}}}{1 + sR_{\text{act,an}}C_{\text{an}}} + \frac{R_{\text{act,ca}}}{1 + sR_{\text{act,ca}}C_{\text{ca}}} \end{aligned} \tag{21}$$

where $R_{\text{act,an}}$ and $R_{\text{act,ca}}$ are incremental resistances depending on operating point current through the electrodes. The impedance response across a spectrum of frequencies is analyzed through Nyquist plot as presented in Fig. 5. The parameters used for the plot are given in Table I. At higher frequencies, the contributions of nonlinear components diminish towards zero, causing the impedance of the electrolyzer to approximate that of a pure resistor. The impedance value varies with the supplied current. This indicates that high-frequency ripples, which are generally produced by power semiconductors have minimal or no effect on the output characteristics of the electrolyzer.

TABLE II: Required Parameters of the Electrolyzer Model

| | | | |
|---|---|---|---|
| $N_{\text{s}}$ | 22 | $A$ | $0.03\,\text{m}^2$ |
| $r_1$ | $59.55 \cdot 10^{-6}\,\Omega\,\text{m}^2$ | $r_2$ | $-340.82 \cdot 10^{-9}\,\Omega\,\text{m}^2\,^\circ\text{C}^{-1}$ |
| $r_3$ | $-106.97 \cdot 10^{-6}\,\Omega\,\text{m}^2\,^\circ\text{C}$ | $r_4$ | $2.71 \cdot 10^{-3}\,\Omega\,\text{m}^2\,^\circ\text{C}^2$ |
| $s_{1,\text{an}}$ | $25.23 \cdot 10^{-3}\,\text{V}$ | $s_{1,\text{ca}}$ | $110.36 \cdot 10^{-3}\,\text{V}$ |
| $s_{2,\text{an}}$ | $-234.03 \cdot 10^{-6}\,\text{V}\,^\circ\text{C}^{-1}$ | $s_{2,\text{ca}}$ | $-1.65 \cdot 10^{-3}\,\text{V}\,^\circ\text{C}^{-1}$ |
| $s_{3,\text{an}}$ | $3.18 \cdot 10^{-6}\,\text{V}\,^\circ\text{C}^{-2}$ | $s_{3,\text{ca}}$ | $22.83 \cdot 10^{-6}\,\text{V}\,^\circ\text{C}^{-2}$ |
| $t_{1,\text{an}}$ | $54.62 \cdot 10^{-3}\,\text{A}$ | $t_{1,\text{ca}}$ | $45.70\,\text{A}$ |
| $t_{2,\text{an}}$ | $-2.46 \cdot 10^{-3}\,\text{A}\,^\circ\text{C}^{-1}$ | $t_{2,\text{ca}}$ | $0.78\,\text{A}\,^\circ\text{C}^{-1}$ |
| $t_{3,\text{an}}$ | $52.12 \cdot 10^{-6}\,\text{A}\,^\circ\text{C}^{-2}$ | $t_{3,\text{ca}}$ | $-10.57 \cdot 10^{-3}\,\text{A}\,^\circ\text{C}^{-2}$ |
| $C_{\text{an}}$ | $0.6373\,\text{F}$ | $C_{\text{ca}}$ | $0.0307\,\text{F}$ |

The supplied current value, $i_{\text{E}}$ influences the behavior of the impedances. As the input current increases, the impact of nonlinear resistances diminishes, leading to a system response that approaches linear ohmic resistance. As shown in Fig. 6, this behavior can be attributed to the fact that higher current levels tend to dominate over the variations introduced by nonlinear elements, effectively reducing their relative contribution to the overall impedance characteristics. The parameters used for plotting the figure have been given in Table II.

Overall, electrolyzers can be characterized as linear systems when operating under conditions of high-frequency and high-current. This characteristic is particularly significant in the context of the dynamic response and overall efficiency of electrolyzers when their current supply is managed by semiconductor-based power converters. Further research is ongoing to investigate the impact of this behavior on the degradation of electrolyzer cells [15]. A more comprehensive multi-physics approach, incorporating factors such as gas production rates and the dynamics of temperature and pressure, may provide valuable insights and help address these questions in future studies.

## V. Model Simulation

The electrical equivalent circuit discussed in Section III is implemented in PLECS to validate its behavior under two static and dynamic operating conditions relevant to both alkaline and PEM electrolyzers. The key parameters necessary for the development and simulation of the model have been extracted from the literature [8] of a $1\,\text{Nm}^3\text{h}^{-1}$ alkaline electrolyzer and has been recorded in Table II. The operating temperature and pressure of the system has been set to $45^\circ\text{C}$ and $25$ bars respectively. The standard reversible voltage has been derived using [16]

$$\begin{aligned} u^0_{\text{rev}} = 1.5184\,\text{V} &- (1.5421 \cdot 10^{-3}\,\text{VK}^{-1})T \\ &+ (9.523 \cdot 10^{-5}\text{VK}^{-1})T \ln T \\ &+ (9.84 \cdot 10^{-8}\text{VK}^{-2})T^2 \end{aligned} \tag{22}$$

The electrolyzer utilizes a potassium hydroxide-based electrolyte, and the saturated vapor pressure has been determined accordingly.

$$p_{\text{sv,E}}(T, m) = 10^{\text{a}} p_{\text{sv}}(T)^{\text{b}} \tag{23a}$$

where a and b are parameters obtained experimentally based on electrolyte type and molality [10].

$$\text{a} = -0.01m - 1.68 \cdot 10^{-3}m^2 + 2.26 \cdot 10^{-5}m^3 \tag{23b}$$

$$\text{b} = 1 - 1.21 \cdot 10^{-3}m + 5.60 \cdot 10^{-4}m^2 - 7.82 \cdot 10^{-6}m^3 \tag{23c}$$

```
// Vapour pressure of pure water
P_v_h2o = exp(81.6179 - (7699.68/T_kelvin) - 10.9*
    log(T_kelvin) + 9.5891*pow(10, -3)*T_kelvin);

//Parameters dependent on KOH solution molal
    concentration
a = -0.0151*m -(1.6788*pow(10, -3)*pow(m, 2)) +
    (2.2588*pow(10, -5)*pow(m, 3));
b = 1 - 1.2062*pow(10, -3)*m + 5.6024*pow(10, -4)*
    pow(m, 2) - 7.8228*pow(10, -6)*pow(m, 3);

//Vapour pressure of KOH solution
P_v_koh = exp(2.302*a + b*log(P_v_h2o));

//Water activity of KOH solution
a_h2o_koh = exp(-0.05192*m + 0.003302*pow(m, 2) +
    (3.177*m - 2.131*pow(m, 2))/T_kelvin);

//Pressure error
e = P - P_v_koh;

//Standard reversible voltage
U_rev_o = 1.5184 - (1.5421*pow(10, -3)*T_kelvin) +
    (9.526*pow(10, -5)*T_kelvin*log(T_kelvin) +
    (9.84*pow(10, -8)*(T_kelvin)));

// Reversible voltage
U_rev = N_s*(U_rev_o + R*T_kelvin*log(e*sqrt(e)/
    a_h2o_koh)/(n_e*F));
```

Listing 1: Code snippet for obtaining total reversible voltage

Listing 1 presents the PLECS C-Scripts utilized to determine the total reversible voltage, using (22), (23a), (23b) and (23c).

First, the electrolyzer model was simulated using a pure DC current of 60 A supplied to the system. This resulted in an output voltage of approximately 34.5 V, which closely aligns with the experimental results presented in [8]. Fig. 7 shows the input current and voltage waveforms. Subsequently, a six-pulse thyristor rectifier was employed as the power supply for the model, with a fixed pulse generation at a firing angle of zero degrees. The input current exhibited an average value of 65 A, resulting in an average output voltage of 34.57 V. As shown in Fig. 8(a), the waveforms exhibit harmonic content. Fig. 8(b) presents the Fourier analysis of the output voltage and current, indicating that 150 Hz harmonics dominate in the current, along with other higher-order harmonics.

## VI. Conclusion

This paper presents a comprehensive electrical model of electrolyzers, designed to capture both their nonlinear characteristics and dynamic behavior. The model is versatile and applicable to various electrolyzer technologies, including alkaline and PEM electrolyzers. Furthermore, it is adaptable to represent emerging electrolyzer technologies with different operational parameters, such as variations in operating points and additional overpotential losses. Frequency response analysis of the total impedance indicates that electrolyzers display resistive behavior at high frequencies. This observation provides valuable insights into their dynamic performance, which is particularly beneficial when power converters are employed as the primary source of electricity for these systems. Finally, the simulation results of the model, performed in PLECS at constant temperature and pressure were validated against the experimental results from the referenced literature, confirming the model's accuracy.

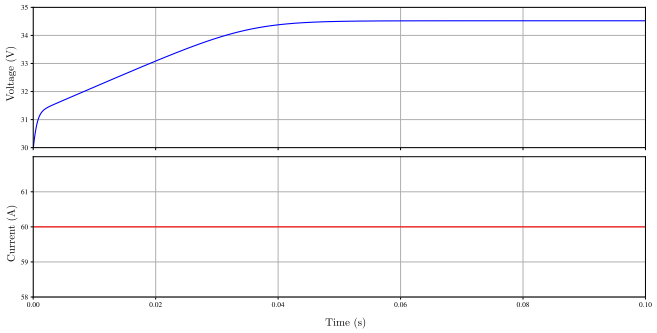


Fig. 7: Simulated voltage and current waveforms when current is supplied from pure DC current source.

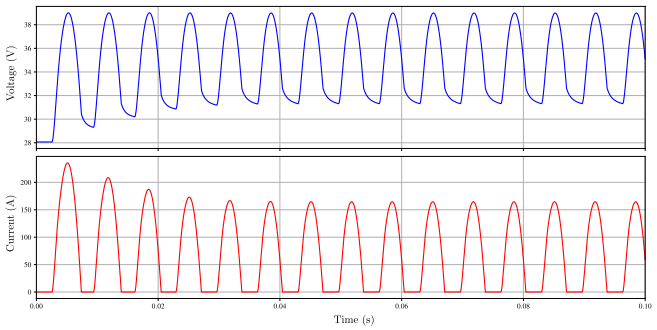


(a)

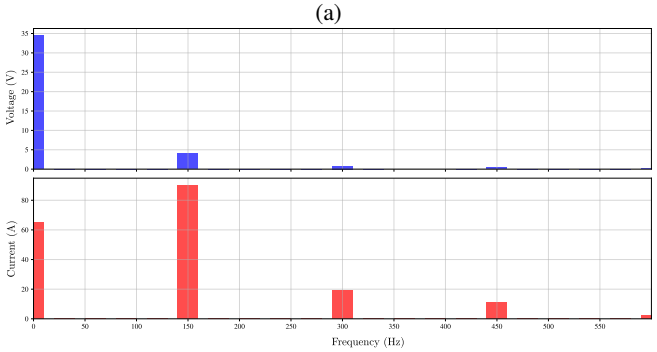


(b)

Fig. 8: Simulated results with current supplied from six-pulse thyristor rectifier (a) Voltage and current waveforms, (b) Fourier analysis of output voltage and current.

## References


[1] International Renewable Energy Agency (IRENA), *Green Hydrogen Strategy: A Guide to Design*. International Renewable Energy Agency, 2024.

[2] European Commission. (2020) A hydrogen strategy for a climate-neutral europe. Accessed: 2024-11-27. [Online]. Available: https://eur-lex.europa.eu/legal-content/EN/TXT/?uri=CELEX:52020DC0301

[3] P. W. Folger, "Hydrogen hubs: Designating locations for clean hydrogen production," Washington, DC, USA, Oct. 2023. [Online]. Available: https://crsreports.congress.gov/product/pdf/R/R48196/2

[4] European Commission. Joint Research Centre., *Clean Energy Technology Observatory, Water electrolysis and hydrogen in the European Union: status report on technology development, trends,*

*value chains and markets : 2023.* LU: Publications Office, 2023. [Online]. Available: https://data.europa.eu/doi/10.2760/133010

[5] *Green hydrogen cost reduction: scaling up electrolysers to meet the 1.5° C climate goal*. Abu Dhabi: Irena, 2020, oCLC: 1413942577.

[6] P. Puranen, M. Hehemann, P. Kütemeier, L. Järvinen, V. Ruuskanen, A. Kosonen, J. Ahola, and P. Kauranen, "Using the Nonlinearity of a Pem Water Electrolyzer Cell for its Dynamic Model Characterization," 2024.

[7] Á. Iribarren, D. Elizondo, E. L. Barrios, H. Ibaiondo, A. Sanchez-Ruiz, J. Arza, P. Sanchis, and A. Ursúa, "Dynamic modeling of a pressurized alkaline water electrolyzer: A multiphysics approach," *IEEE Transactions on Industry Applications*, vol. 59, no. 3, pp. 3741–3753, 2023.

[8] A. Ursúa and P. Sanchis, "Static–dynamic modelling of the electrical behaviour of a commercial advanced alkaline water electrolyser," *International Journal of Hydrogen Energy*, vol. 37, no. 24, pp. 18 598–18 614, 2012, 2011 International Workshop on Molten Carbonates & Related Topics.

[9] J. Koponen, V. Ruuskanen, A. Kosonen, M. Niemelä, and J. Ahola, "Effect of converter topology on the specific energy consumption of alkaline water electrolyzers," *IEEE Transactions on Power Electronics*, vol. 34, no. 7, pp. 6171–6182, 2019.

[10] L. Järvinen, P. Puranen, A. Kosonen, V. Ruuskanen, J. Ahola, P. Kauranen, and M. Hehemann, "Automized parametrization of pem and alkaline water electrolyzer polarisation curves," *International Journal of Hydrogen Energy*, vol. 47, no. 75, pp. 31 985–32 003, 2022.

[11] H. R. Corti, "Polymer electrolytes for low and high temperature PEM electrolyzers," *Current Opinion in Electrochemistry*, vol. 36, p. 101109, Dec. 2022. [Online]. Available: https://linkinghub.elsevier.com/retrieve/pii/S2451910322001740

[12] S. Shiva Kumar and V. Himabindu, "Hydrogen production by pem water electrolysis – a review," *Materials Science for Energy Technologies*, vol. 2, no. 3, pp. 442–454, 2019.

[13] M. El-Shafie, "Hydrogen production by water electrolysis technologies: A review," *Results in Engineering*, vol. 20, p. 101426, 2023.

[14] D. C. Grahame, "The Electrical Double Layer and the Theory of Electrocapillarity." *Chem. Rev.*, vol. 41, no. 3, pp. 441–501, Dec. 1947, publisher: American Chemical Society. [Online]. Available: https://doi.org/10.1021/cr60130a002

[15] S. Schumann, T. Runser, F. Herzig, and B. Craciun, "Water electrolysis power supply," in *Components of Power Electronics and their Applications 2023: ETG Symposium*, 2023, pp. 122–128.

[16] R. L. LeRoy, C. T. Bowen, and D. J. LeRoy, "The thermodynamics of aqueous water electrolysis," *Journal of The Electrochemical Society*, vol. 127, no. 9, p. 1954, sep 1980. [Online]. Available: https://dx.doi.org/10.1149/1.2130044